On the Generation of Exact Solutions for Evaluating Numerical Schemes and Estimating Discretization Error

Christopher J. Roy*

Aerospace and Ocean Engineering Department, Virginia Polytechnic Institute and State University, VA 24061, USA

Andrew J. Sinclair

Aerospace Engineering Department, Auburn University, AL 36849, USA

CORRESPONDING AUTHOR

Dr. Chris Roy
Associate Professor
Aerospace and Ocean Engineering Dept.
215 Randolph Hall
Virginia Tech
Blacksburg, VA 24061-0203
Voice: (540) 231-0080
FAX: (540) 231-9632
Email: cjroy@vt.edu

Note: A preliminary version of this paper was presented at the NATO-RTO AVT-147 Symposium on Computational Uncertainty in Military Vehicle Design, Athens, Greece 3-4 December 2007.

ABSTRACT

In this paper we further develop the Method of Nearby Problems (MNP) for generating exact solutions to realistic partial differential equations by extending it to two dimensions. We provide an extensive discussion of the 2D spline fitting approach which provides C^k continuity (continuity of the solution value and its first *k* derivatives) along spline boundaries and is readily extendable to higher dimensions. A detailed one-dimensional example is given to outline the general concepts, then the two-dimensional spline fitting approach is applied to two problems: heat conduction with a distributed source term and the viscous, incompressible flow in a lid-driven cavity with both a constant lid velocity and a regularized lid velocity (which removes the strong corner singularities). The spline fitting approach results in very small spline fitting errors for the heat conduction problem and the regularized driven cavity, whereas the fitting errors in the standard lid-driven cavity case are somewhat larger due to the singular behaviour of the pressure near the driven lid. The MNP approach is used successfully as a discretization error estimator for the driven cavity cases, outperforming Richardson extrapolation which requires two grid levels. However, MNP has difficulties with the simpler heat conduction case due to the discretization errors having the same magnitude as the spline fitting errors.

Keywords: exact solution, discretization error, spline fit, defect correction, computational fluid dynamics

1. INTRODUCTION

High-fidelity computational simulations are playing an ever-increasing role in the design and development of engineering systems. It is thus critical to be able to quantify the uncertainty in the simulation predictions. Numerical error is an important factor in the overall uncertainty in the simulation prediction. A key component of the uncertainty is the explicit numerical error in the prediction itself. In addition, numerical error plays a more subtle role when significant numerical errors are present during the model validation phase. If too large, these numerical errors can yield "false positives" for the validation of the model. Furthermore, if large numerical errors are present during a model calibration step, then these errors will have propagated into the model.

There are three components of the numerical error: round-off error, iterative error, and discretization error [1]. Round-off error can be mitigated by simply using more significant digits in the computation. Iterative error can often be reduced by simply running additional iterations or monitoring convergence of the solution residuals. Discretization error is the most difficult aspect of numerical error to analyze, and is defined as the difference between the exact solution to the discretized equations and the exact solution to the original partial differential equations (PDEs). Assuming iterative and round-off errors are negligible relative to the discretization error, the numerical solution can be used as a surrogate for the exact solution to the discrete equations when estimating the discretization error.

The main difficulty in estimating the discretization error is finding a way to estimate the exact solution to the PDEs. Exact solutions exist for only the simplest equations or simplified versions of nonlinear, coupled partial differential equations. The most common way of estimating the exact

solution to the PDEs is Richardson extrapolation [2], which uses numerical solutions on two or more grids to estimate the exact solution. Richardson extrapolation requires uniform refinement over the entire domain, and that both of the mesh levels be in the asymptotic grid convergence regime where errors are reduced at the rate dictated by the formal order of accuracy of the method (e.g., the rate found by evaluating the truncation error). A third grid is needed to confirm that the asymptotic regime has been reached. The requirement for three grid levels (all in the asymptotic regime) is difficult to achieve both because of the total number of grid points required and the burden on the grid generation tool to generate uniformly refined grids. Another promising approach for estimating discretization errors is the adjoint method [3]. While this approach can provide estimates of the discretization error in any quantity of interest, there is a great deal of overhead associated with the coding and solving of the adjoint system. This approach is thus very difficult from a code development point of view. Furthermore, adjoint methods have not yet been demonstrated for realistic engineering problems on complex geometries.

Recently, an approach for estimating discretization error has been proposed by our group called the Method of Nearby Problems (MNP) [4]. MNP requires two numerical solutions on the same grid, thereby eliminating the problems associated with generating multiple grids that are all within the asymptotic grid convergence regime. The steps associated with applying MNP as a single-grid discretization error estimator are:

1. compute the original numerical solution on the chosen grid,
2. generate an accurate curve fit to this numerical solution, thereby providing an analytic representation of the numerical solution,

3. operate the governing partial differential equations on the curve fit from step 2 to generate small analytic source terms,
4. compute the nearby problem (original problem plus analytic source terms) on the chosen grid,
5. evaluate the exact discretization error (i.e., numerical solution minus the analytic curve fit) on the nearby problem, and
6. assume that the discretization error in the nearby problem can be used to estimate the discretization error in the original problem of interest.

The key point to this approach is that, by definition, the curve fit generated in step 2 is the exact solution to the nearby problem. If the source terms are sufficiently small, then the nearby problem is said to be sufficiently near the original problem. This technique is loosely related to the Method of Manufactured Solution for code verification [2]; however, in the present case, the solution must be a realistic solution (which is not a requirement for Manufactured Solutions). MNP is related to a type of defect correction technique known as differential correction (for more information see the review by Skeel [5]).

MNP has been successfully demonstrated for one-dimensional problems [4]. Roy et al. used MNP to estimate discretization errors in steady-state Burgers equation for viscous shocks. They used 5th order Hermite splines to generate the exact solutions for Reynolds numbers of 8, 64, and 512. MNP was found to provide equivalent error estimates to extrapolation-based methods, but with the advantage of using only a single grid level. Global Legendre polynomial fits for steady-state Burgers equation for a viscous shock at a Reynolds number of 16 are given in Fig. 1a. Not only is the viscous shock wave not adequately resolved, but the global fits also exhibit significant oscillations at the boundaries. Hermite spline fits for an even higher Reynolds number of 64 are given in Fig. 1b, with

the spline fit in very good agreement with the underlying numerical solution. For a detailed discussion on the "goodness" of the spline fits, see Ref. [4].

The purpose of the current paper is to extend the MNP approach of Roy et al. from 1D to 2D. The difficult task of generating a spline fit which is C^k continuous (i.e., the solution is continuous up to k derivatives) along the entire spline boundary is first discussed. Then two examples are given which demonstrate the effectiveness of the 2D spline fitting procedure: steady-state heat conduction with a distributed heat source (Poisson's equation) and incompressible, viscous flow in a lid-driven cavity (the Navier-Stokes equations). MNP is also applied as an error estimator to both problems. Both sets of governing equations contain second derivatives, so C^3 continuous spline fits are used to provide source terms which will be continuous in both the value and slope across spline boundaries. The use of different levels of continuity is not examined in this paper.

2. SPLINE FITTING APPROACH

Here we extend the one-dimensional spline fitting procedure to two dimensions using the weighting function approach of Junkins et al. [6], which uses a series of overlapping local curve fits $Z_n(x,y)$ which are joined together with higher-order weighting functions $W_n(x,y)$. In two dimensions, the fitting function for a local region can be written as:

$$Z(x,y) = \sum_{n=1}^{4} Z_n(x,y) \cdot W_n(\bar{x},\bar{y})$$

where the n index represents different fitting regions for the local curve fits and the overbars indicate that the independent variables in the weighting functions are normalized to go from zero to one on each local region, i.e.,

$$0 \le \bar{x} \le 1, \quad \text{and} \quad 0 \le \bar{y} \le 1$$

The basis functions for these local curve fits Z_n can be chosen as needed, and thus can be modified to handle regions containing strong gradients or singularities. The weighting functions W_n are chosen such that an arbitrary level of continuity can be enforced between the fitting regions (function value, first derivative, second derivatives, etc.). In addition, these weighting functions ensure that the contribution from the local curve fits goes to zero at the boundaries of their local regions of applicability. For two-dimensional flows, these weighting functions are chosen such that the functions W_2, W_3, and W_4 are simple coordinate transformations of W_1:

$$\begin{aligned} W_2(\bar{x},\bar{y}) &= W_1(1-\bar{x},\bar{y}) \\ W_3(\bar{x},\bar{y}) &= W_1(1-\bar{x},1-\bar{y}) \\ W_4(\bar{x},\bar{y}) &= W_1(\bar{x},1-\bar{y}) \end{aligned}$$

Additional constraints used to determine the form of the weighting functions in 2D are that the weighting function W_1 and its k-derivatives must equal zero along the two lines $\bar{x} = 0$ and $\bar{y} = 0$, it must equal unity at ($\bar{x} = 1$, $\bar{y} = 1$), and the sum of the weighting functions must be equal to unity

$$\sum_{n=1}^{4} W_n(\bar{x},\bar{y}) = 1$$

for all $0 \le \bar{x} \le 1$ and $0 \le \bar{y} \le 1$. For example, for C^1 continuity (i.e., continuity of the function value and its first derivative) at local fitting boundaries, the weighting function W_1 is

$$W_1(\bar{x},\bar{y}) = \bar{x}^2\bar{y}^2\left(9 - 6\bar{x} - 6\bar{y} + 4\bar{x}\bar{y}\right)$$

and the form for C^3 continuity (used for all of the current results) is

$$\begin{aligned} W_1(\bar{x},\bar{y}) = \bar{x}^4\bar{y}^4(&1225 - 2940\bar{y} + 2450\bar{y}^2 - 700\bar{y}^3 - 2940\bar{x} + 7056\bar{x}\bar{y} - 5880\bar{x}\bar{y}^2 + 1680\bar{x}\bar{y}^3 \\ &+ 2450\bar{x}^2 - 5880\bar{x}^2\bar{y} + 4900\bar{x}^2\bar{y}^2 - 1400\bar{x}^2\bar{y}^3 - 700\bar{x}^3 + 1680\bar{x}^3\bar{y} - 1400\bar{x}^3\bar{y}^2 + 400\bar{x}^3\bar{y}^3) \end{aligned}$$

where again $\bar{x}$ and $\bar{y}$ are linearly scaled to vary between zero and one in each region. These two weighting functions are shown graphically in Fig. 2 and are essentially one quadrant of a three-dimensional bell shape with a square base. Although possibly not unique, the general form of the weighting function for C^k continuity is:

$$W_1^k(\bar{x},\bar{y}) = \bar{x}^{k+1}\bar{y}^{k+1}\sum_{i=0}^{k}\sum_{j=0}^{k} a_{i,j}\bar{x}^i\bar{y}^j$$

where the $a_{i,j}$ coefficients are found using the constraints given above. It should be noted that once the series of local fits has been generated, they can be joined together with weighting functions of varying degree of continuity in order to provide the best overall fit on the domain.

A simple 1D example of this weighting function approach is presented in Fig. 3, where the original data used to generate the spline fit are simply 17 points sampled at equal intervals from the function $\sin(2\pi x)$. The goal of this example is to create a spline fit made up of four spline regions which exhibits C^2 continuity at the spline zone interfaces. The first step is to generate five

overlapping local fits Z_1 through Z_5, with each of the interior fits spanning two spline regions (see top of Fig. 3). Here a least squares method is used to find a best fit quadratic function in each of the five regions:

$$Z_n(\bar{x}) = a_n + b_n \bar{x} + c_n \bar{x}^2$$

Since each spline zone now has two different local fits, one from the left and the other from the right, these two local fits are combined together with the left and right weighting functions shown in Fig. 3 (middle). The form of the 1D weighting function used here for C^2 continuity is

$$W_{RIGHT}(\bar{x}) = \bar{x}^3\left(10 - 15\bar{x} + 6\bar{x}^2\right)$$

and recall that $W_{LEFT}(\bar{x}) = W_{RIGHT}(1-\bar{x})$. Thus the final fit in each region can be written as

$$F(x,y) = W_{LEFT} Z_{LEFT} + W_{RIGHT} Z_{RIGHT}$$

For example, for region 2, one would have $Z_{LEFT} = Z_2$ and $Z_{RIGHT} = Z_3$. Note that in addition to providing the desired level of continuity at spline boundaries, the weighting functions are also useful in reducing the dependence on the extreme ends of the local fits where they often exhibit the poorest agreement with the original data. When these final fits are plotted (bottom of Fig. 3), we see that they are indeed C^2 continuous, maintaining continuity of the function value, slope, and curvature at all three interior spline boundaries.

3 RESULTS

3.1 2D Heat Conduction

The first problem of interest is two-dimensional heat conduction with a distributed heat source term. Assuming a constant thermal conductivity, the steady-state energy equation can be written as

$$\frac{\partial^2 T}{\partial x^2} + \frac{\partial^2 T}{\partial y^2} = s(x, y)$$

where *s(x,y)* represents a spatially distributed heating source. This source term is found by choosing the following exact solution, similar to the method of manufactured solutions:

$$\widetilde{T}(x, y) = T_0 + T_{xy} \sin\left(\frac{a_{xy} \pi x^2 y^2 (1-x)^2 (1-y)^2}{L^8} \right)$$

This problem is solved on the domain $0 \le x \le 1\,\text{m},\ 0 \le y \le 1\,\text{m}$ using the following constants:

$$T_0 = 300\ \text{K}, \quad T_{xy} = 50\ \text{K}$$
$$a_{xy} = 192, \quad L = 1\,\text{m}$$

The resulting source term can be easily found by operating the Laplace operator onto this solution. The argument of the sine function in the solution is chosen to provide a constant temperature and zero temperature gradient along the four boundaries. A simple explicit symmetric Gauss-Seidel finite difference discretization is used which is second-order accurate. The numerical solution on a 257×257 grid is shown graphically in Fig. 4a and exhibits a strong temperature gradient as well as significant curvature of the temperature profiles.

The 2D weighting function approach was used to generate a spline fit based on the 257×257 node numerical solution. Bi-cubic polynomials of the form

$$F(x,y) = \sum_{i=0}^{3}\sum_{j=0}^{3} c_{i,j} x^i y^j$$

were employed for the local least squares fits, and the C^3 continuous 2D weighting functions given above were used to assemble these local fits. The bi-cubic basis functions were chosen as reasonable functions to fit the solution which has non-constant curvature. The resulting spline fit using only 8×8 spline zones is given in Fig. 4b and qualitatively captures all of the features found in the underlying numerical solution. A more quantitative analysis of the "goodness" of the spline fits is shown in Fig. 5 which gives the discrete L_1, L_2, L_∞ norms of the difference between the spline fit and the underlying numerical solution. The average spline fitting error magnitude (L_1 norm) over the entire domain is less than 0.01 *K* for 8×8 spline zones and less than 2×10^{-6} *K* for 64×64 spline zones. The maximum spline fitting error magnitude (L_∞ norm) is less than 0.08 *K* for 8×8 spline zones and nearly 1×10^{-5} *K* for 64×64 spline zones. The spline fitting errors are proportional to one over the number of spline zones to the fourth power, thus doubling the number of spline zones reduces the spline fitting errors by a factor of 16. Note that since the total number of unknowns in the local least squares fit is 16, the maximum number of spline zones in each directions is limited to a factor of four less than the maximum number of nodes in each direction (e.g., for the 65×65 node mesh, the maximum number of spline zones is 16×16). Thus there is a trade-off when using higher order basis functions because fewer spline zones may be used.

The local variation in the spline fitting error for this case is given in Fig. 6a and 6b for 8×8 and 64×64 spline zones, respectively. The maximum error magnitudes are 0.08 *K* for 8×8 zones and 1×10^{-5} *K* for 64×64 spline zones. It is clear that by increasing the number of spline zones, the error in the spline fit is substantially reduced. Another approach for reducing the spline fitting error is to increase the order of the polynomial fit for each of the local curve fits; however, this latter approach was not investigated in the current work.

MNP can also be used to estimate the discretization error in 2D heat conduction problem by assuming the error in the nearby problem (which we can evaluate exactly) is very close to that of the original problem. In this case, the 33×33 node numerical solution was fit using the above procedure using 4×4 spline zones, where bi-cubic local fits are used with C^3 continuous weighting functions. The estimated discretization error (numerical solution to the nearby problem minus the exact solution to the nearby problem, i.e., the spline fit) is presented below in Fig. 7a, along with the true error (numerical solution to the original problem minus the exact solution to the original problem), the Richardson extrapolation error estimation method (see Ref. [2]), and the error in the spline fit itself. For this case, MNP does not estimate the true error nearly as well as Richardson extrapolation. This heat transfer case is a difficult case for MNP because the solution contains large gradients and curvature, but elliptic problems are generally easy ones for achieving the asymptotic grid convergence regime. This supposition is supported by the fact that the spline fitting errors for this case are on the same order as the discretization error we are trying to estimate, as shown in Fig. 7a. Furthermore, when a spline fit is generated based on a finer underlying numerical solution (65×65)

with additional spline zones (16×16), the nearby problem does indeed provide accurate error estimates on the 33×33 node mesh as shown in Fig. 7b.

3.2 2D Viscous Incompressible Flow

The second example problem is the viscous, incompressible flow in a lid-driven cavity at a Reynolds number of 100. This flow can be described by a modified form of the incompressible Navier-Stokes equations, which for constant transport properties are given by

$$\frac{1}{\rho\beta^2}\frac{\partial p}{\partial t}+\frac{\partial u}{\partial x}+\frac{\partial v}{\partial y}=S_2+S_4$$

$$\rho\frac{\partial u}{\partial t}+\rho u\frac{\partial u}{\partial x}+\rho v\frac{\partial u}{\partial y}-\frac{\partial p}{\partial x}=\mu\frac{\partial^2 u}{\partial x^2}+\mu\frac{\partial^2 u}{\partial y^2}$$

$$\rho\frac{\partial v}{\partial t}+\rho u\frac{\partial v}{\partial x}+\rho v\frac{\partial v}{\partial y}-\frac{\partial p}{\partial y}=\mu\frac{\partial^2 v}{\partial x^2}+\mu\frac{\partial^2 v}{\partial y^2}$$

These equations are solved in finite-difference form on a co-located (i.e., non-staggered) Cartesian mesh by integrating in pseudo-time using Chorin's artificial compressibility method [7]. In order to suppress odd-even decoupling (a common problem when solving the incompressible Navier-Stokes equations on non-staggered grids [8]), second- and fourth-derivative pressure damping (S_2 and S_4, respectively) are added to the mass conservation equation

$$S_2=C_2\Delta x\frac{\left|p_{i+1,j}-2p_{i,j}+p_{i-1,j}\right|}{\left|p_{i+1,j}+2p_{i,j}+p_{i-1,j}\right|+\varepsilon}\frac{\partial^2 p}{\partial x^2}+C_2\Delta y\frac{\left|p_{i,j+1}-2p_{i,j}+p_{i,j-1}\right|}{\left|p_{i,j+1}+2p_{i,j}+p_{i,j-1}\right|+\varepsilon}\frac{\partial^2 p}{\partial y^2}$$

$$S_4=\frac{1}{4}\rho C_4\Delta x^2\frac{\partial^4 p}{\partial x^4}+\frac{1}{4}\rho C_4\Delta y^2\frac{\partial^4 p}{\partial y^4}$$

where $C_2 = 1.0$, $C_4 = -1\times10^{-4}$, and $\varepsilon = 1\times10^{-10}$ unless otherwise noted. This fourth derivative pressure damping is similar to that employed by Sotiropoulos and Abdallah [9]. This modified form of the equations reduces to the steady-state incompressible Navier-Stokes equations in the limit as the mesh is refined and as a steady-state solution is obtained. Dirichlet boundary conditions are used for velocity (all velocities are zero except for the *u*-velocity is set to unity at the top wall) and the boundary pressure is found from the interior solution.

3.2.1 Driven Cavity

A contour plot of the *u*-velocity (i.e., the velocity in the *x*-direction) from a numerical solution on a 257×257 grid is given in Fig. 8a. Also shown in the figure are streamlines which denote the overall clockwise circulation induced by the upper wall velocity (the upper wall moves from left to right), as well as the two counter-clockwise rotating vortices in the bottom corners. A spline fit was generated using 3rd order polynomials with C^3 continuous weighting functions and 64×64 spline zones. Note that while no additional boundary constraints are placed on the velocity components for the spline fit, the maximum deviations from the original boundary conditions are on the order of 1×10^{-7} m/s and are thus quite small. The *u*-velocity contours and streamlines for the spline fit are presented in Fig. 8b. As was found before for the 2D heat conduction case, the fit solution is qualitatively the same as the underlying numerical solution. The streamlines were injected at exactly the same locations in both figures and are indistinguishable from each other. Furthermore, in both cases the streamlines near the center of the cavity follow the same path for multiple revolutions.

One of the difficulties that arises in both solving the driven cavity problem and in generating spline fits of the resulting solutions is the presence of strong singularities at the two top corners

where the moving lid meets the stationary walls. The flow stagnation in the top right corner leads to a strong pressure rise, while the flow acceleration in the top left corner leads to a strong pressure drop. Contours of static (gauge) pressure for the 257×257 numerical solution are given in Fig. 9a, while contours for the spline fit using 64×64 zones are shown in Fig. 9b. Again, these contours are qualitatively identical.

A more quantitative comparison between the underlying numerical solution and the spline fits is presented in Fig. 10 which shows the spline fitting error relative to the numerical solution as a function of the number of spline zones in each direction. For the *u*-velocity (Fig. 10a), the average error magnitude (L_1 norm) decreases from 1×10^{-3} m/s to 3×10^{-6} m/s with increasing number of spline zones from 8×8 to 64×64, while the maximum error (L_∞ norm) decreases from 0.7 m/s to 0.01 m/s. For the static pressure (Fig. 10b), the average error magnitude decreases from 1×10^{-3} N/m^2 to 5×10^{-6} N/m^2 with increasing number of spline zones, while the maximum error decreases from 1 N/m^2 to nearly 0.01 N/m^2.

In addition to using the spline fitting approach to generate exact solutions, MNP has been employed to estimate the discretization error in the original driven cavity numerical solution. As discussed previously, if the nearby problem is "near enough" to the original problem of interest, then the discretization error in the nearby problem (which can be evaluated exactly) can serve as an estimate of the error in the original problem of interest. The estimated discretization error at the mid-height of the cavity using MNP for the 65×65 nodes solution is presented in Fig. 11 along with error estimates from Richardson extrapolation (which also requires the solution on a coarser 33×33 node mesh). In order to judge which error estimation approach is more accurate, a numerical solution is

also computed on a very fine 257×257 nodes mesh, with the resulting solution used to approximate the "true error" which is displayed as symbols in Fig. 11. The discretization error estimates using MNP are generally not as good as those from Richardson extrapolation when the nominal value of the second-derivative damping coefficient ($C_2 = 1.0$) is used in the nearby problem; however, as this coefficient is reduced to 0.1 and then ultimately to zero (i.e., no second-derivative damping), the error estimates from MNP improve dramatically and are somewhat better than those found from Richardson extrapolation. In this case the nearby problem is likely smoother than the original problem, especially near the singular corners. Thus the nearby problem does not require the second derivative damping (whereas the original problem was unstable without some second derivative damping). In addition, these damping terms act as additional terms in the governing equations which are being neglected when computing the source term for the nearby problem. Table 1 gives the maximum difference between the different discretization error estimates and the true error as judged by the "truth" mesh, which can also be considered as the error in the error estimate. While Richardson extrapolation consistently out-performs MNP, as the second-derivative damping coefficient (C_2) is reduced, the error estimates from MNP are significantly improved relative to Richardson extrapolation.

Contour plots of the discretization error in the *v*-velocity are presented in Fig. 12 for a) the "true" error (approximated using the 257×257 node mesh), b) MNP with $C_2 = 0$, and c) Richardson extrapolation. The MNP approach clearly provides a more accurate representation of the true error in the center of the cavity; however, Richardson extrapolation does appear to be more accurate near the two corner singularities.

3.2.2 Regularized Cavity

A simpler Navier-Stokes case is generated by gradually reducing the lid velocity at the two ends of the lid. The lid velocity profile for this so-called regularized cavity is set to be

$$u(x, y = y_{\max}) = \frac{1}{2} U_{lid} \left[1 + \sin\left(\frac{2\pi x}{L} - \frac{\pi}{2} \right) \right]$$

where it is assumed that $0 \le x \le L$ (here L = 0.05 m). For the regularized cavity, the second-derivative damping coefficient was reduced to 0.1.

Contours of u-velocity and streamlines for the regularized cavity on a 257×257 node mesh are given in Fig. 13a, and it is evident that the corner singularities have been removed. A spline fit was generated for this case using 3rd order polynomials, C^3 continuous weighting functions, and 64×64 spline zones. The resulting u-velocity contours and streamlines are given in Fig. 13b and are indistinguishable from those in the original problem.

A more quantitative comparison of the underlying solution and subsequent spline fit can be found by examining norms of the spline fitting errors. Spline fitting error norms are presented in Fig. 14 for a 257×257 node numerical solution for varying number of spline zones for a) the u-velocity and b) the pressure. These error norms are 2-3 orders of magnitude lower than those seen for the standard driven cavity, suggesting that the regularization process makes it much easier to generate

accurate spline fits. For 64×64 spline zones, the maximum errors over the domain for u-velocity and pressure were found to be approximately 5×10^{-5} m/s and 6×10^{-5} N/m^2, respectively.

MNP is employed as a discretization error estimator for the regularized cavity on a grid of 65×65 nodes, and the estimated errors in *u*-velocity, *v*-velocity, and pressure at the cavity mid-height are given in Fig. 15. All of the error estimation strategies compare well with the "truth mesh," which is again found by simply solving the original problem on a very fine 257×257 node mesh. In addition, minimal effects are seen when the second-derivative damping coefficient C_2 is set to zero. Contour plots of the estimated discretization error in the *v*-velocity are given in Fig. 16 for a) the truth mesh, b) MNP, and c) Richardson extrapolation. Again, both error estimation methods provide good error estimates. The maximum error magnitudes in the discretization error estimates are given in Table 2 for the regularized cavity case, with MNP providing mixed results relative to the Richardson extrapolation approach.

4 CONCLUSIONS

An approach was presented, based on earlier work by Junkins et al. [6], for generating 2D spline fits which provide and arbitrary level of continuity at spline boundaries. This approach was discussed in detail and was applied to two 2D problems: steady-state heat conduction and incompressible flow in a lid-driven cavity. The spline fitting approach was able to generate accurate fits of the numerical solutions, with the "goodness" of the fit increasing as additional spline zones were added. By operating the original continuous governing equations onto these spline fits, modified governing equations which include small, analytic source terms were generated. The advantage to solving these

modified equations is that the exact solution is available. The approach thus provides exact solutions to problems "nearby" the original governing equations (i.e., they differ only by the small, analytic source terms).

In addition to the generation of exact solutions, the approach was further applied to estimate the discretization error in the original problem. The main idea here is that if the nearby problem is sufficiently "near" to the original problem of interest, then the discretization error in the Nearby Problem (which can be evaluated exactly and does not need to be estimated) can serve as an estimate of the discretization error on the original problem of interest. Discretization error estimates were made for both the heat conduction problem and the driven cavity (both with a constant lid velocity and a regularized lid velocity) and were compared with Richardson extrapolation. The MNP approach did not provide accurate estimates of the discretization error for the heat conduction problem because the spline fitting errors, although small, were on the same order of magnitude as the discretization error. This scenario is not the case for more realistic problems, and indeed MNP provided accurate error estimates for the two driven cavity cases, comparable to or better than those found from Richardson extrapolation (which requires multiple grid levels).

While these initial 2D results are promising, there are still some unresolved issues that are beyond the scope of the current work. First, the nearness of the Nearby Problem must be quantified in a more rigorous manner, possibly through the use of appropriate norms of the derivatives of the solution (i.e., Sobolev norms). This could also mitigate the high frequency oscillations seen in the spline fitting errors for the heat conduction case (Fig. 6). In addition, an area for further investigation is the optimal application of the spline-fitting approach (i.e., the selection of basis functions, the

order of weighting functions, and the number of spline zones) for use in MNP. The MNP approach could easily be extended to stretched curvilinear meshes by implementing a discrete mesh transformation (i.e., performing the spline fitting in computational space), but the extension of the approach to unstructured meshes is not clear. Finally, a major advantage of the current approach is that it is readily extendable to arbitrary levels of continuity and to higher dimensions.

ACKNOWLEDGEMENTS

We would like to thank Matthew Hopkins of Sandia National Laboratories for the many helpful discussions on the Method of Nearby Problems. This work was supported by a grant from Sandia National Laboratories through a U.S. Department of Energy Presidential Early Career Award for Scientists and Engineers with Dr. Matthew Barone serving as technical monitor. Sandia is a multiprogram laboratory operated by Sandia Corporation, a Lockheed Martin Company, for the United States Department of Energy's National Nuclear Security Administration under contract DE-AC04-94AL85000.

REFERENCES

[1] C. J. Roy, "Review of Code and Solution Verification Procedures for Computational Simulation," *Journal of Computational Physics*, Vol. 205, No. 1, 2005, pp. 131-156.

[2] P. J. Roache, *Verification and Validation in Computational Science and Engineering*, Hermosa Publishers, New Mexico, 1998.

[3] D. A. Venditti and D. L. Darmofal, "Anisotropic Grid Adaptation for Functional Outputs: Application to Two-Dimensional Viscous Flows," *Journal of Computational Physics*, Vol. 187, No. 1, 2003, pp. 22-46.

[4] C. J. Roy, A. Raju, and M. M. Hopkins, "Estimation of Discretization Errors using the Method of Nearby Problems," *AIAA Journal*, Vol. 45, No. 6, June 2007 (see also A. Raju, C. J. Roy, and M. M. Hopkins, "Evaluation of Discretization Error Estimators using the Method of Nearby Problems," AIAA Paper 2005-4993, 2005).

[5] R. D. Skeel, "Thirteen Ways to Estimate Global Error," *Numerische Mathematik*, Vol. 48, No. 1, 1986, pp. 1-20.

[6] J. L. Junkins, G. W. Miller, and J. R. Jancaitis, "A Weighting Function Approach to Modeling of Irregular Surfaces," *Journal of Geophysical Research*, Vol. 78, No. 11, April 1973, pp. 1794-1803.

[7] A. J. Chorin, "A Numerical Method for Solving Incompressible Viscous Flow Problems," *Journal of Computational Physics*, Vol. 2, No. 1, 1967, pp. 12-26.

[8] D. Tafti, "Alternate Formulations for the Pressure Equation Laplacian on a Collocated Grid for Solving the Unsteady Incompressible Navier-Stokes Equations," *Journal of Computational Physics*, Vol. 116, No. 1, 1995, pp. 143-153.

[9] F. Sotiropoulos and S. Abdallah, "The Discrete Continuity Equation in Primitive Variable Solutions of Incompressible Flow," *Journal of Computational Physics*, Vol. 95, No. 1, 1991, pp. 212-227.

TABLES

Table 1. Maximum error magnitude in the discretization error estimate for the driven cavity case

	RE	MNP	MNP (C2=0.1)	MNP (C2=0.0)
u-velocity	33%	66%	15%	8%
v-velocity	14%	32%	10%	16%
Pressure	20%	28%	6%	8%

Table 2. Maximum error magnitude in the discretization error estimate for the regularized cavity case

	RE	MNP (C2=0.1)	MNP (C2=0.0)
u-velocity	1.7%	5.7%	5.7%
v-velocity	7.8%	5.2%	6.1%
Pressure	10%	17%	17%

FIGURES

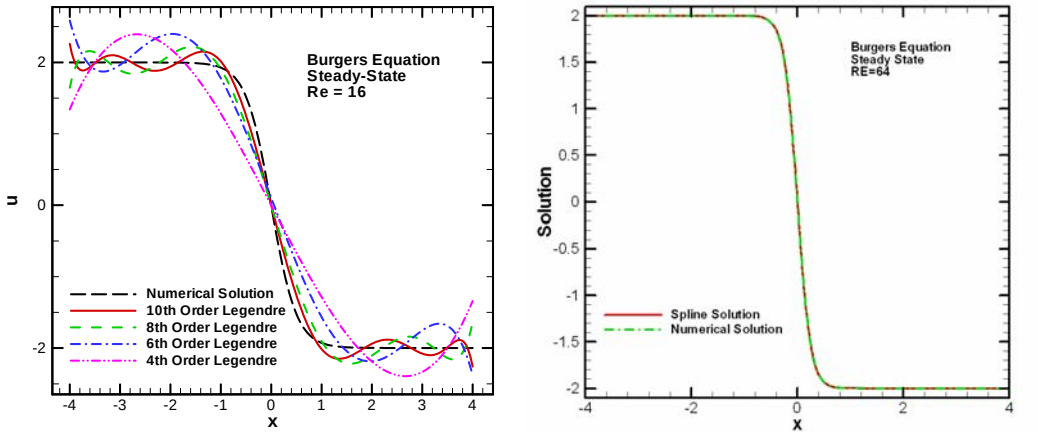

a) b)

Figure 1: Examples of curve fitting for the viscous shock wave solution to Burgers equation: a) global Legendre polynomial fits for Re = 16 and b) 5th order Hermite splines for Re = 64

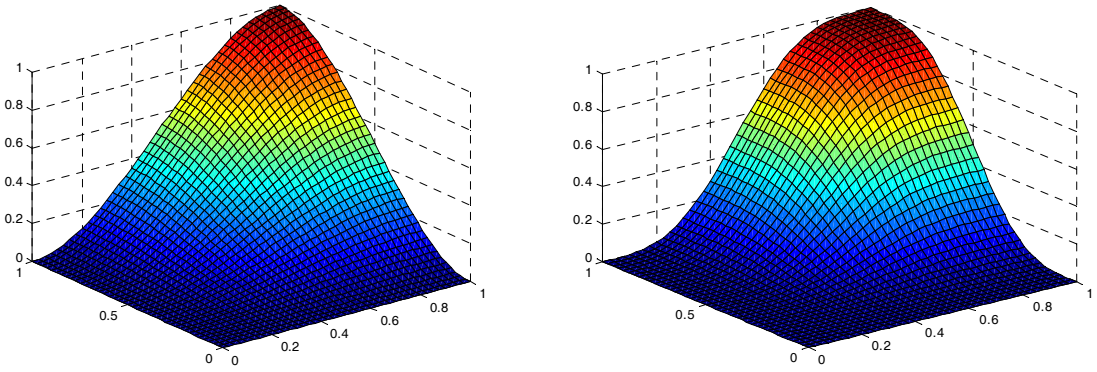

a) b)

Figure 2: Weighting functions $W_1(\bar{x},\bar{y})$ for a) C^1 continuity and b) C^3 continuity

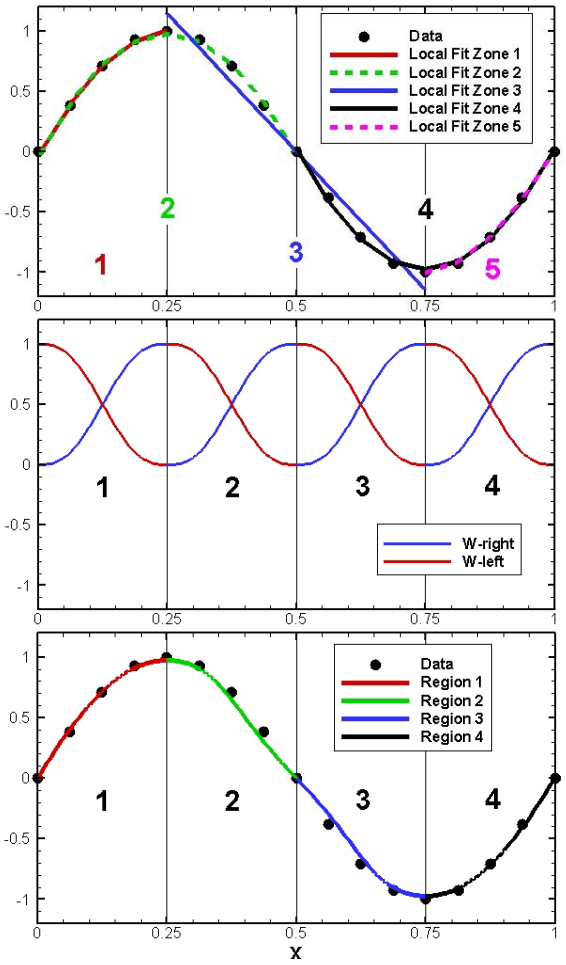

Figure 3: Simple one-dimensional example of the weighting function approach for combining local quadratic least squares fits to generate a C^2 continuous spline fit: local fits (top), weighting functions (middle), and resulting C^2 continuous spline fit (bottom)

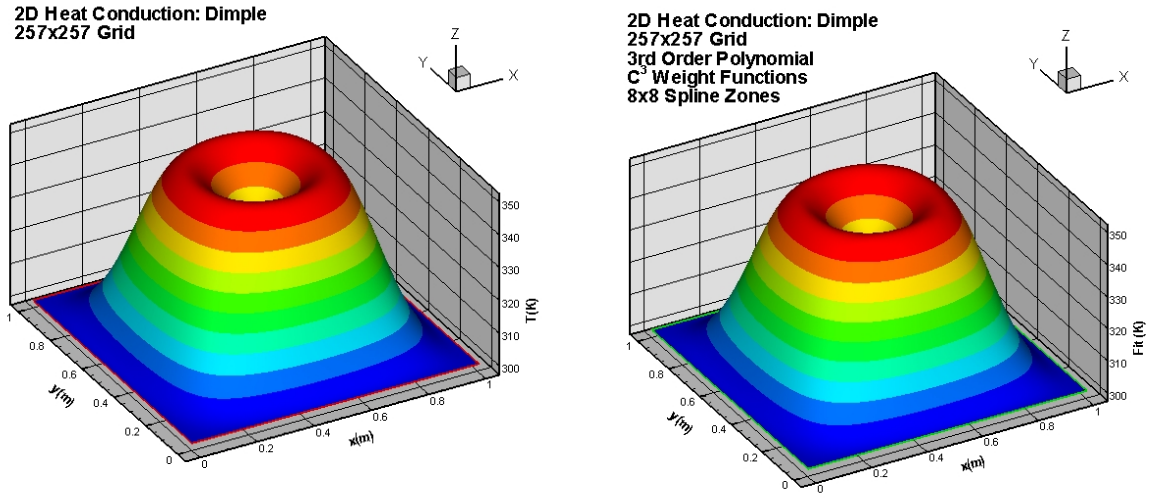

a) b)

Figure 4: Two-dimensional heat conduction with a distributed source: a) numerical solution on a 257x257 node mesh and b) C^3 continuous spline fit using 8x8 spline zones

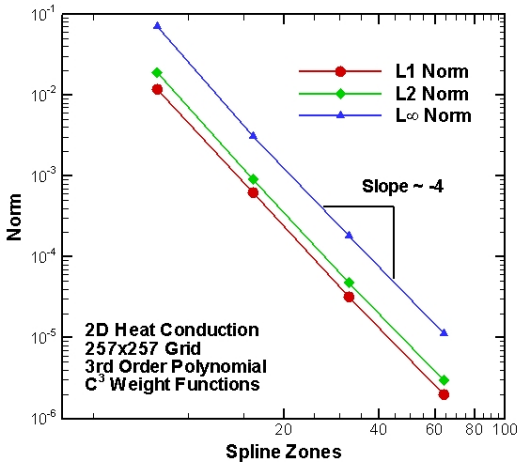

Figure 5: Variation of the error between the spline fits and the underlying 257x257 node numerical solution as a function of the number of spline zones in each direction

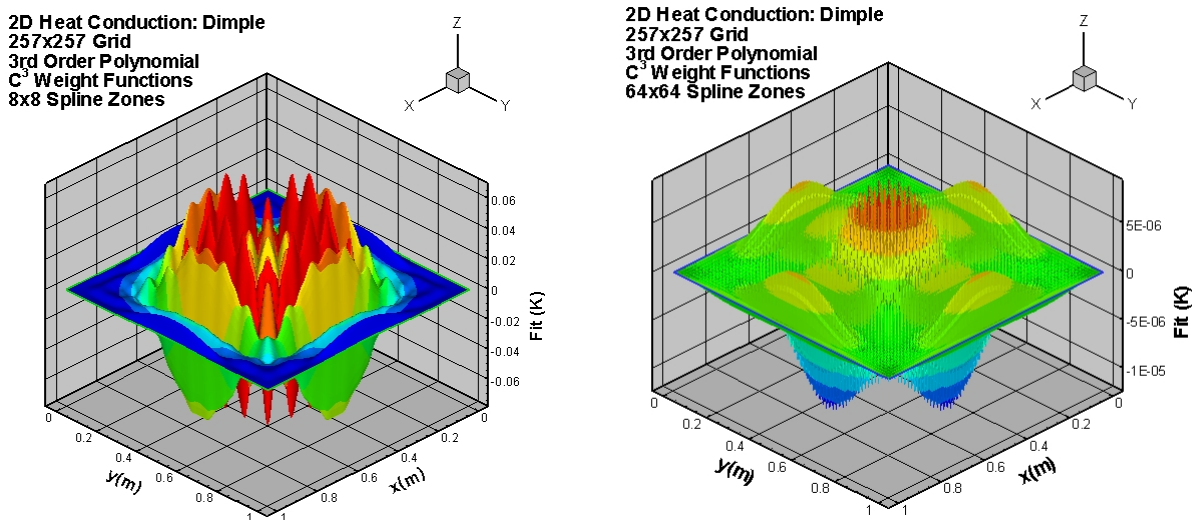

a) b)

Figure 6: Local distributions of the spline fitting error relative to the 257x257 node underlying numerical solution: a) 8x8 spline zones and b) 64x64 spline zones

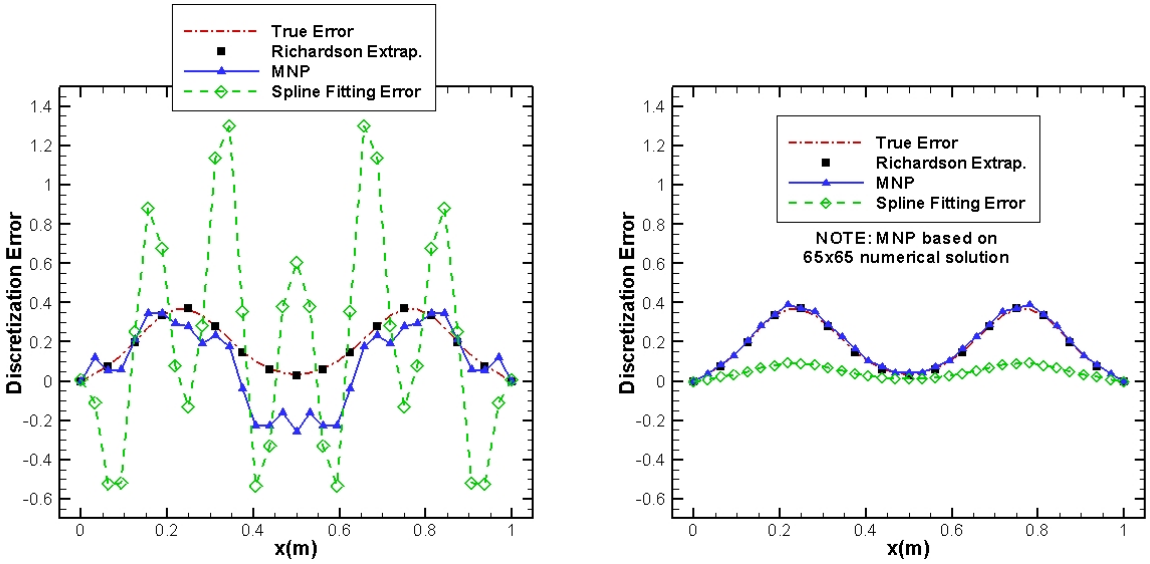

a) b)

Figure 7: Discretization error estimates for the 33x33 node heat conduction solution comparing MNP to Richardson extrapolation and the true error using a) 4x4 spline zones based on the 33x33 solution and b) 16x16 spline zones based on the 65x65 solution; also shown is the error in the spline fit

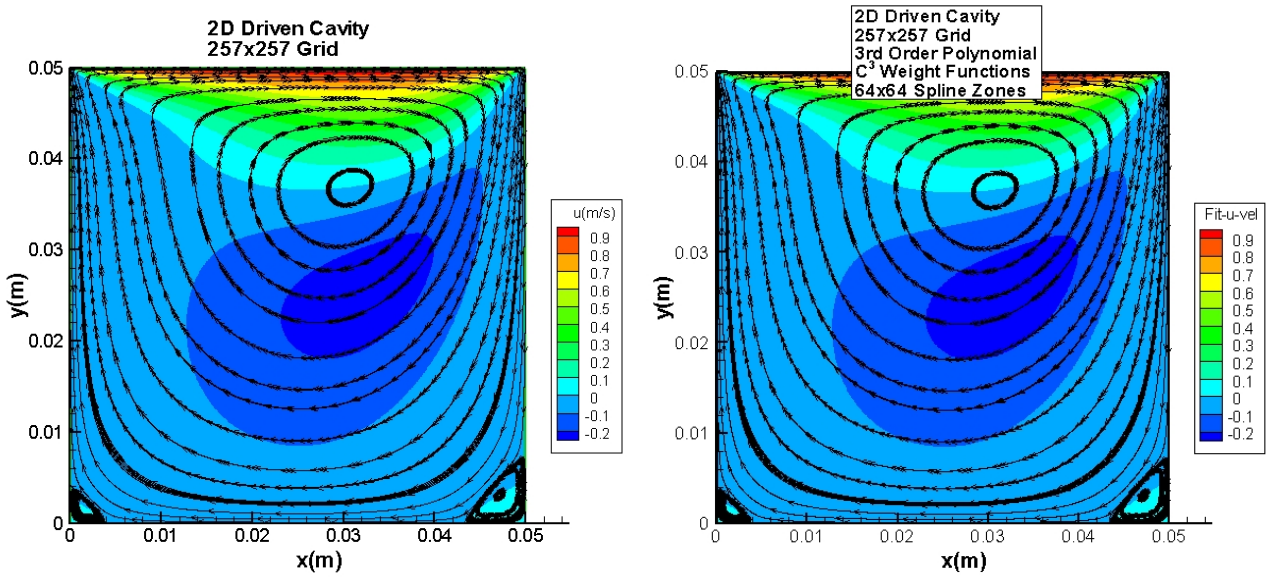

a) b)

Figure 8: Contours of *u*-velocity and streamlines for the driven cavity case at Reynolds number 100: a) 257x257 node numerical solution and b) C^3 continuous spline fit using 64x64 spline zones

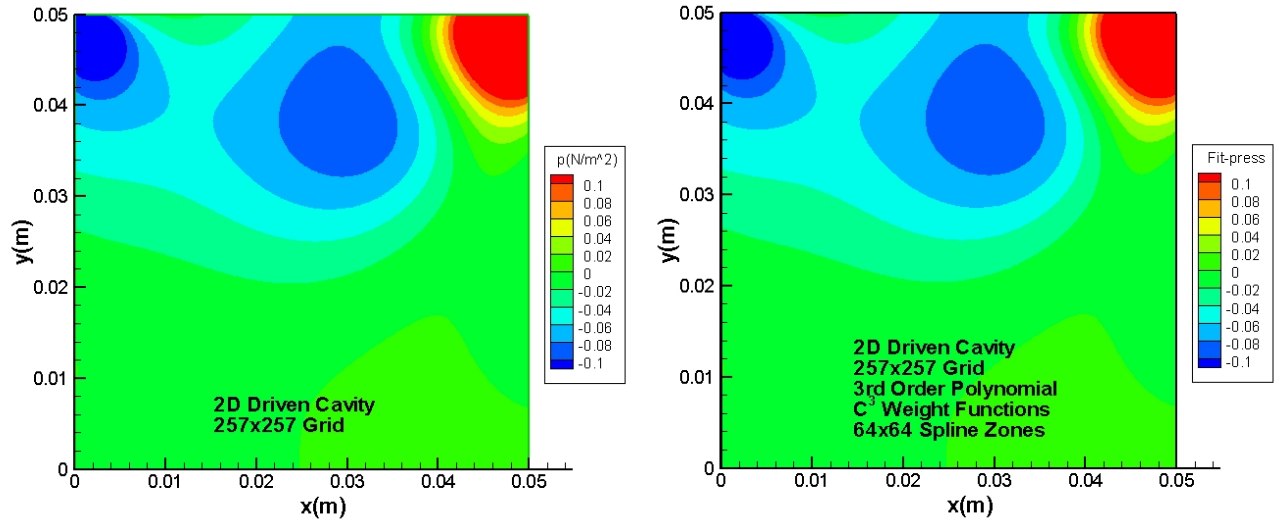

a) b)

Figure 9: Contours of static gauge pressure for the driven cavity case at Reynolds number 100: a) 257x257 node numerical solution and b) C^3 continuous spline fit using 64x64 spline zones

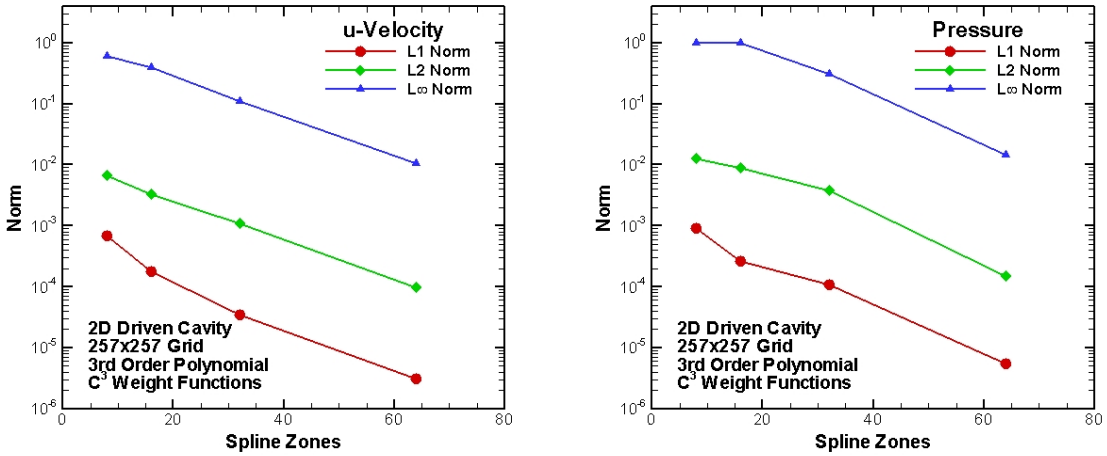

a) b)

Figure 10: Variation of the error between the spline fits and the underlying 257x257 numerical solution as a function of the number of spline zones in each direction for the driven cavity: a) *u*-velocity and b) pressure

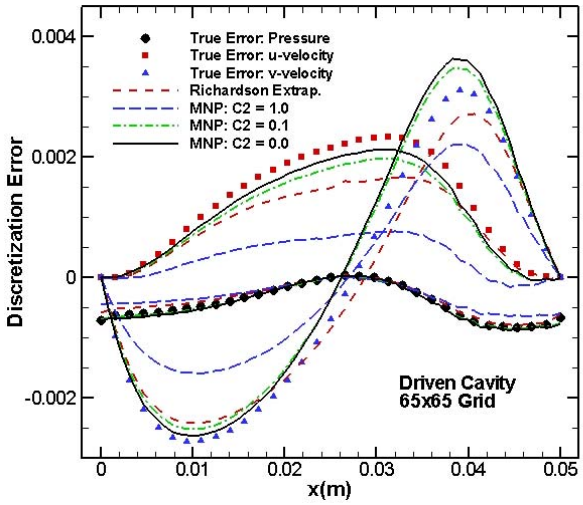

Figure 11: Discretization error for the standard driven cavity along the line y = 0.025 m (cavity centerline) showing the true error (estimated from a 257x257 grid), Richardson extrapolation (using grids of 65x65 and 33x33 nodes), and MNP using varying second-derivative damping constants

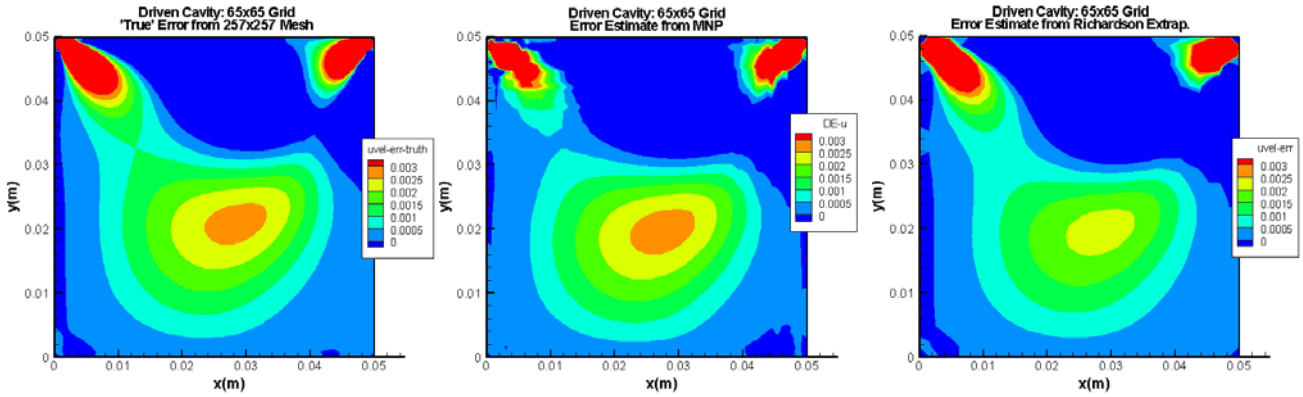

a) b) c)

Figure 12: Contours of the discretization error in *u*-velocity for the standard driven cavity: a) true error estimated from a 257x257 grid, b) error estimate from the MNP procedure with C_2 = 0.0, and c) error estimate from Richardson extrapolation

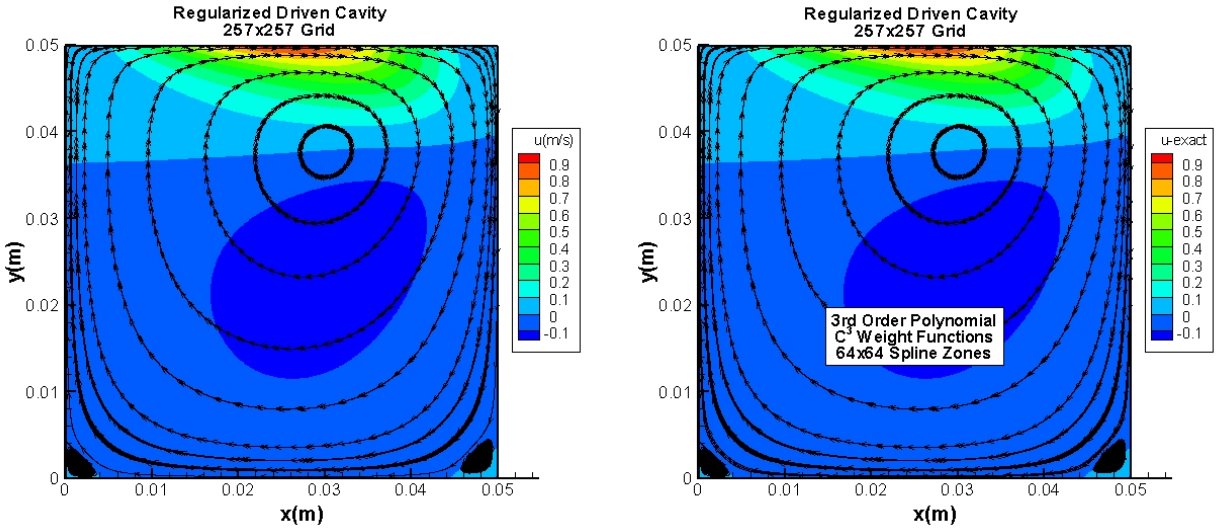

a) b)

Figure 13: Contours of *u*-velocity and streamlines for the regularized driven cavity: a) original numerical solution on 257x257 nodes and b) nearby solution on 257x257 nodes using 64x64 spline zones

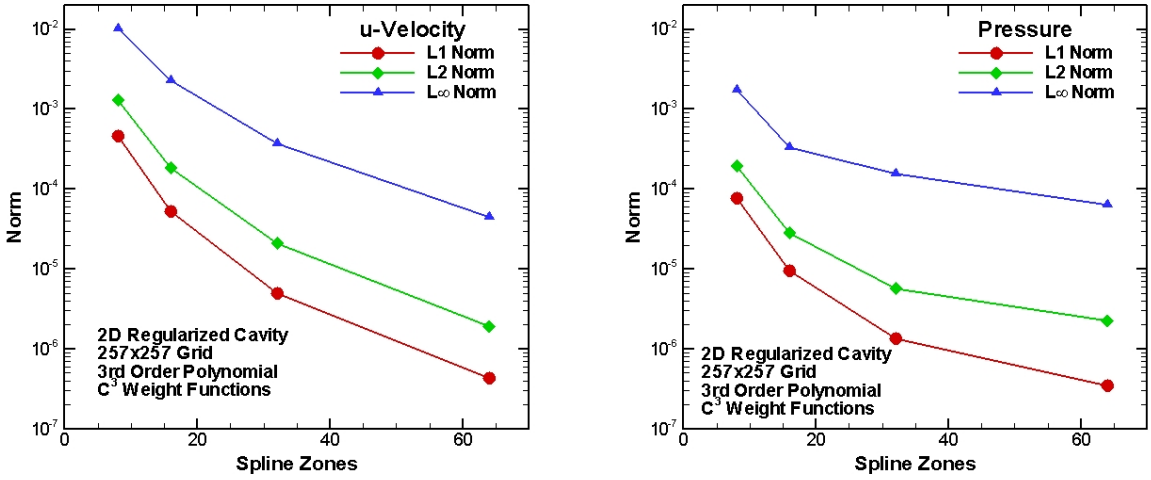

a) b)

Figure 14: Variation of the error between the spline fits and the underlying 257x257 numerical solution as a function of the number of spline zones in each direction for the regularized cavity: a) *u*-velocity and b) pressure

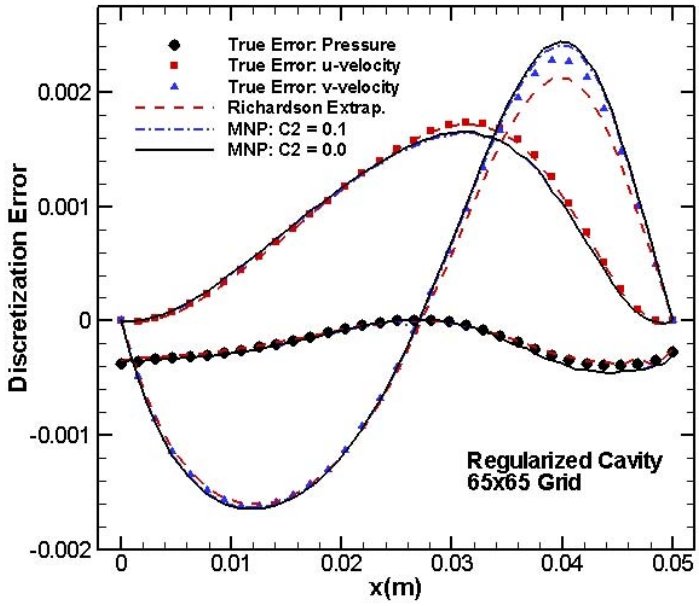

Figure 15: Spline fit fitting error for the regularized driven cavity along the line y = 0.025 m (cavity centerline) showing the true error (estimated from a 257x257 grid), Richardson extrapolation, and MNP

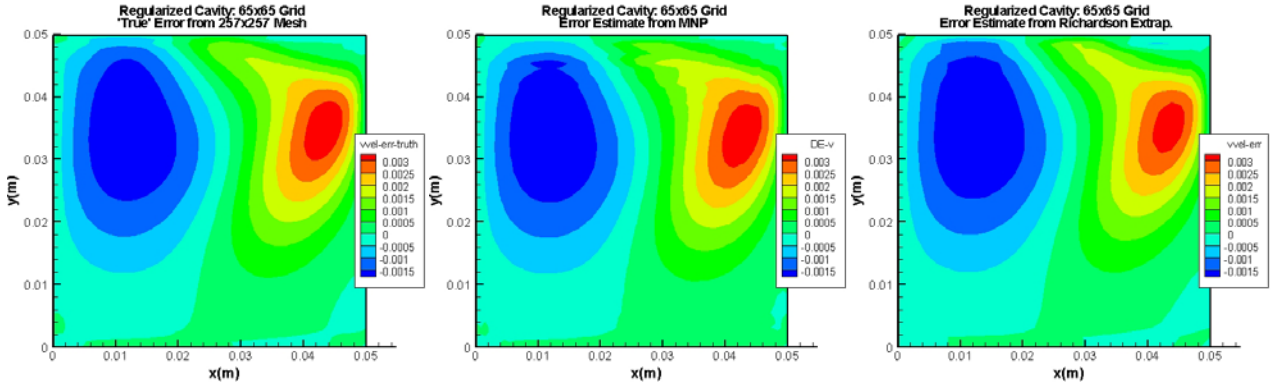

a) b) c)

Figure 16: Contours of the discretization error in *v*-velocity for the regularized driven cavity: a) true error estimated from a 257x257 grid, b) error estimate from the MNP procedure with C_2 = 0.0, and c) error estimate from Richardson extrapolation